



Large-scale arsenic mobilization from legacy sources in anoxic aquifers: Multiple methods and multi-decadal perspectives

Feifei Cao^{a,*}, Dan B. Kleja^{b,c}, Charlotta Tiberg^c, Jerker Jarsjö^a

^a Department of Physical Geography, Bolin Center for Climate Research, Stockholm University, SE-106 91 Stockholm, Sweden

^b Department of Soil and Environment, Swedish University of Agricultural Sciences (SLU), Box 7014, SE-750 07 Uppsala, Sweden

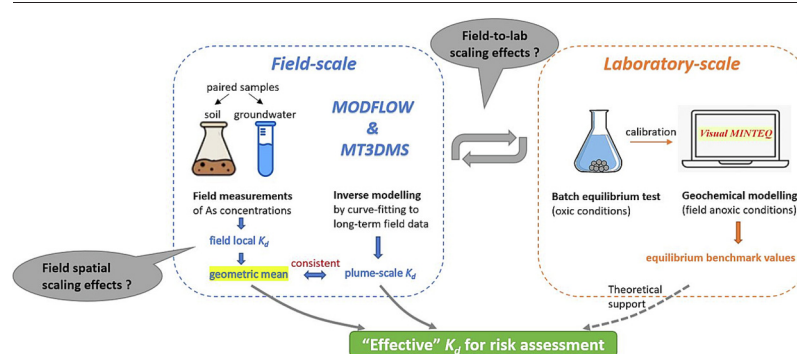
^c Swedish Geotechnical Institute (SGI), SE-581 93 Linköping, Sweden



HIGHLIGHTS

- Geometric mean of local K_d values gives best estimates of field effective K_d .
- Geochemical modelling provides a unique understanding of As retention mechanisms.
- Field-spatial scaling effects highlight within-site subsurface heterogeneities.
- Laboratory-to field scaling effects highlight sampling and measurement issues.

GRAPHICAL ABSTRACT



ARTICLE INFO

Editor: Deyi Hou

Keywords:

Arsenic mobilization
 Anthropogenic source
 Soil pollution
 Groundwater contamination
 Solid-liquid partition
 Risk assessment

ABSTRACT

While geogenic arsenic (As) contamination of aquifers have been intensively investigated across the world, the mobilization and transport of As from anthropogenic sources have received less scientific attention, despite emerging evidence of poor performance of widely used risk assessment models. In this study we hypothesize that such poor model performance is largely due to insufficient attention to heterogeneous subsurface properties, including the hydraulic conductivity K and the solid-liquid partition (K_d), as well as neglect of laboratory-to-field scaling effects. Our multi-method investigation includes i) inverse transport modelling, ii) in-situ measurements of As concentrations in paired samples of soil and groundwater, and iii) batch equilibrium experiments combined with (iv) geochemical modelling. As case study we use a unique 20-year series of spatially distributed monitoring data, capturing an expanding As plume in a Chromated Copper Arsenate (CCA)-contaminated anoxic aquifer in southern Sweden. The in-situ results showed a high variability in local K_d values of As (1 to 107 L kg⁻¹), implying that over-reliance of data from only one or few locations can lead to interpretations that are inconsistent with field-scale As transport. However, the geometric mean of the local K_d values (14.4 L kg⁻¹) showed high consistency with the independently estimated field-scale “effective K_d ” derived from inverse transport modelling (13.6 L kg⁻¹). This provides empirical evidence for the relevance of using geometric averaging when estimating large-scale “effective K_d ” values from local measurements within highly heterogeneous, isotropic aquifers. Overall, the considered As plume is prolonged by about 0.7 m year⁻¹, now starting to extend beyond the borders of the industrial source area, a problem likely shared with many of the world’s As-polluted sites. In this context, geochemical modelling assessments, as presented here, provided a unique understanding of the processes governing As retention, including local variability in, e.g., Fe/Al-(hydr)oxides contents, redox potential and pH.

* Corresponding author.

E-mail address: feifei.cao@natgeo.su.se (F. Cao).

1. Introduction

Arsenic (As) is a ubiquitous contaminant in soil and groundwater and is recognized as a worldwide problem due to its significant risk to public health. High concentrations of geogenic As in groundwater have been reported in many regions around the world, particularly in some large river deltas in Southeast Asia (e.g., Charlet et al., 2007; van Geen et al., 2008; Wallis et al., 2020). The behavior of geogenic As in soil and groundwater has been intensively studied over the last two decades, due to its wide occurrence, its complex chemistry and the serious threat it poses to drinking water resources (e.g., Guo et al., 2014; Mariner et al., 1996; O'Day et al., 2004; Stopelli et al., 2020). In addition, agricultural, mining, industrial activities as well as hazardous waste disposal have introduced large amounts of anthropogenic As into the environment, which might leach to groundwaters and aquatic environments (Carraro et al., 2015; Chatain et al., 2005; Ganne et al., 2006; Nadiri et al., 2018; Sbarbati et al., 2020). Mobilization of As might be also triggered by introducing anthropogenic organic carbon into aquifers, e.g. at landfills (Keimowitz et al., 2005) and petroleum-impacted sites (Cozzarelli et al., 2016). Industrial use of chromated copper arsenate (CCA) is one of the major anthropogenic sources of As in soil and aquatic environments (Morais et al., 2021; Nriagu et al., 2007). CCA has been utilized in the wood impregnation industry since the 1930s and became increasingly popular in the late 1980s (Saxe et al., 2007). Although restrictions have been imposed on the use of As in wood preservation since the early 2000s (e.g. European Commission Directive 2003/2/EC), the legacy of such sources still pose important threats to the environment (Hopp et al., 2006; Morais et al., 2021; Smedley and Kinniburgh, 2013). Whereas a large number of studies have concerned geogenic As, investigations related to impacts of anthropogenic As including CCA-contaminated hotspots are less frequent and have mainly focused on laboratory-scale leaching and mobilization studies (e.g., Andersen et al., 1996; Jang et al., 2002; Nakiguli et al., 2020).

A key issue related to anthropogenic As contamination is whether or not, and at which pace, contaminant plumes may develop in groundwater downstream of the original spatially limited source area. For instance, a systematic evaluation of hundreds of sites severely contaminated by metals (including As; Augustsson et al., 2020) showed generally poor performance of models that assessed the risk of exceeding regulatory limit values for groundwater quality. In natural groundwaters, As mainly occurs in inorganic As(III) or As(V) form, with the more mobile As(III) prevailing under anoxic conditions and less mobile As(V) predominating in oxic waters (Oremland and Stolz, 2003; Smedley and Kinniburgh, 2002). One major factor governing As mobility is sorption, leading to retardation of As compared to groundwater flow. Low sorption and high As mobility is associated with risk of development of lengthy plumes downstream of the original source zones. This implies aggravation of environmental impacts from anthropogenic As sources over time, which additionally may be accelerated by climate change effects (Jarsjö et al., 2020). Sorption can be assessed by the solid-liquid partitioning (K_d). A common approach is to assume a linear sorption isotherm, i.e. the constant K_d approach, which is frequently applied due to its simplicity and easy integration into various models (Degryse et al., 2009; Stockmann et al., 2017). The constant K_d is calculated as the ratio of the solid-phase concentration to the liquid-phase concentration, where the solid-phase concentration is represented either by the total As concentration (Mariner et al., 1996; Yang et al., 2012) or by the “exchangeable” As concentration estimated by extraction with phosphate (Guo et al., 2014; van Geen et al., 2008) or oxalate (Davies, 2022).

To determine K_d values for As, the most widely used methods include measurements of As concentration in paired samples of solid-phase material and groundwater (e.g., Ni et al., 2016; van Geen et al., 2008) and/or laboratory batch equilibrium tests (e.g., Blaisi et al., 2019; Jung et al., 2012). However, K_d values are highly dependent on geochemical properties, including solid-phase (e.g., content of Fe and Al hydroxides) and liquid-phase properties (e.g., pH, redox potential). The K_d value will therefore be “conditional” and change with time if conditions change. Furthermore, in contrast to coupled reactive transport models (e.g. Stolze et al.,

2019), the K_d approach gives no information on the reaction mechanism (s) involved in controlling the solubility of an element (surface complexation, mineral precipitation/dissolution etc.). In this respect, geochemical models (e.g., equilibrium models MINTEQA2, Visual MINTEQ) can be used as complementary tools to support K_d evaluations, by revealing the underlying solubility control mechanisms. Alternatively, geochemical equilibrium models can be used to generate realistic “conditional” K_d values applicable to the geochemical conditions prevailing at the study site of interest.

Due to heterogeneous geochemical and hydrogeological properties of the subsurface, K_d values and As retention may exhibit considerable within-site spatial variabilities (Michael and Khan, 2016). Differences in geochemical conditions may generate K_d values which differ by orders of magnitude (Smedley and Kinniburgh, 2002). Also, possible geological stratification (layering) of aquifers and the random presence of high-permeability structures (e.g., macro-pores that greatly enhance water flows) will determine the large-scale hydraulic conductivity (K) of the aquifers as well as the transport properties of substances in the aquifers. As a result, the large-scale “effective K_d ”, which represents the overall As retention in the aquifer, may differ considerably from the local K_d values derived from laboratory-scale studies. This hence raises questions regarding sample representativeness and systematic scale differences. However, in heterogeneous aquifers, such effective values of K and K_d may instead be derived from inverse modelling of substance breakthrough curves (concentration-time series) obtained by groundwater measurements downstream of a source area (U.S. EPA, 1999). In contrast to laboratory tests, such an inverse approach will yield an “effective K_d ” for the whole site or aquifer, incorporating both hydrogeological and geochemical heterogeneities that commonly are well hidden from observation.

In this study, we hypothesize that heterogeneities in subsurface properties in the field may lead to considerable differences in local K_d values and As retention. These spatial, temporal and laboratory-to-field scaling effects have rarely been clarified in scientific literature to date, and may prevent robust risk assessments of contaminated sites. We also hypothesize that a better understanding of such scaling effects would support the robust estimation of an “effective K_d ” representative of entire aquifers. To test these hypotheses, addressing also the robustness of alternative estimation methods, we used a multi-method approach to derive different estimates of “effective K_d ” values for As in an anoxic aquifer, by combining data from local soil and groundwater measurements, batch experiments, chemical equilibrium modelling, and field-scale inverse transport modelling. A CCA-contaminated site in southern Sweden with in-situ observations of As plume development over a 20-year period was selected as case study area. The main objectives were 1) to evaluate a multi-methodology for K_d estimation for As at a pollution hotspot, 2) to assess the main hydrogeological and geochemical parameters influencing the long-term (multi-decadal) transport of As in the aquifer, and 3) to determine a representative K_d value for field scale transport of As taking into account spatial, temporal and laboratory-to-field scaling effects.

2. Site description

2.1. Location and hydrogeological context

The CCA site is a former wood preservation plant located in Hjältevad in southern Sweden (Fig. 1). The facility covers an area of approximately 5.3 ha, largely surrounded by residential buildings except for some forested land to the east. Lake Hjälte and River Brusaån are located about 300 m north of the facility, with the latter flowing from the lake in the west to the northeast of the area. The facility was built on an almost flat ground with an altitude of about +168 m a.s.l. (RH 2000). The bedrock consists of granite, with depths ranging from about 18 to 38 m. The soil consists mainly of glaciofluvial deposits, that were gradually built up in layers of sand, gravel and silt. Sand is the dominant fraction at all levels, with the proportion of coarse sand decreasing with depth and the proportion of fine sand and silt increasing with depth. This has been confirmed by drill

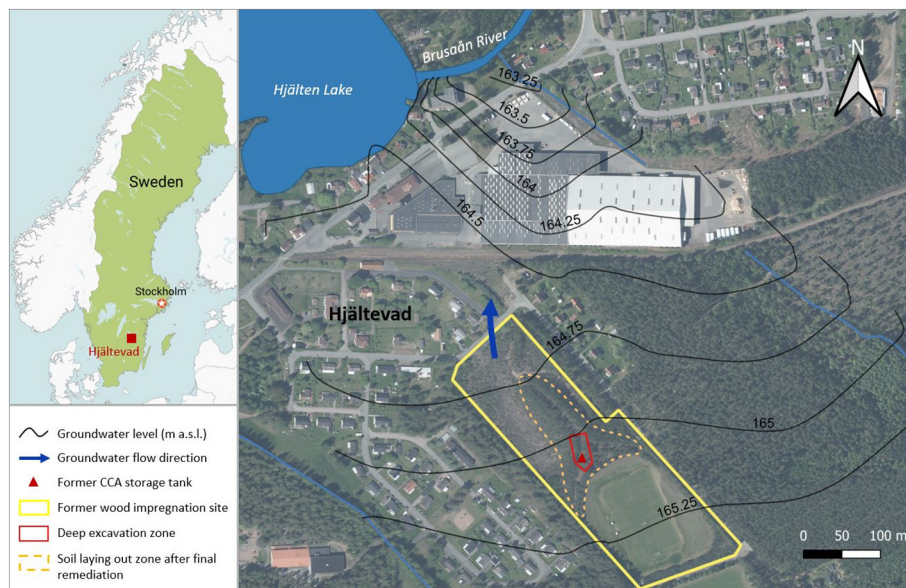


Fig. 1. Location and hydrogeological map of the study area.

core sampling at the study area, showing gradually decreasing grain size of the soil with depth (see details in Supplementary, section 1).

The aquifer is a shallow unconfined aquifer located within the glaciofluvial sediments, with an average groundwater depth of approximately 3 m (+165 m a.s.l.) at the former wood preservation facility (Fig. 1). A groundwater level contour map produced by triangulation based on groundwater level measurements in the study area (Fig. 1) shows that the aquifer is naturally drained by the Brusån River and that the groundwater flow has a general northwestern direction. The climate in the region is warm and temperate with an average annual temperature of 6.3 °C and an average annual precipitation of 700 mm, according to values for the period 1991–2020 from Swedish Meteorological and Hydrological Institute (SMHI).

2.2. Arsenic in the study area

The dominant CCA product used at the impregnation plant throughout its operating period (from 1949 to 1985) was Boliden K33, which contained 34.0 % of As_2O_5 , 26.6 % of CrO_3 , 14.8 % of CuO and 24.6 % of water. The major impregnation equipment was located in the center of the facility, with a large underground steel tank for the storage of CCA solution (Fig. 1). The tank was in use until a leak was discovered in 1968, which constitutes the main source of As pollution in soil and groundwater. In addition, contaminants have also spread through spills and drips from the impregnation equipment and/or from the impregnated products along transport routes and in storage areas. However, while significant amounts of CCA reached the aquifer due to the leak, the spills and drips have mainly impacted the upper soil layers. After the leakage was discovered in 1968, attempts were made to remediate the area using the “pump and treat” method from 1968 to 1993. Additionally, remediation was carried out in 1997 by an *on-site* ex-situ soil washing method. The surface soil was excavated in layers of 0.1 m until As concentrations did not exceed 40 mg kg^{-1} . Around the storage tank, the soil was excavated to a depth of 10 m below the ground surface within an area of approximately 800 m^2 (Fig. 1). Excavated soil with As content $>40 \text{ mg kg}^{-1}$ was treated in a soil washing plant. The deep excavated zone was backfilled with uncontaminated soil. Washed soil, together with excavated soil containing low levels of As ($<40 \text{ mg kg}^{-1}$) were deposited on the remediated site, laying out a hill reaching a height of 5–7 m above the original ground surface (Fig. 1).

After the soil washing in 1997, a continuous rise of As concentration in groundwater has been observed from a monitoring well (TB8) downstream the former CCA storage tank (Fig. 2), indicating a considerable residual

pollution in the former hotspot area. Monitoring based on a network of 39 observation wells from 2017 to 2021 has identified a large pollution plume of about $20,000 \text{ m}^2$ with groundwater As concentration $>10 \mu\text{g L}^{-1}$. The current source zone with As content in solid material above 50 mg kg^{-1} includes the area around, below and immediately downstream the deep excavated zone (Fig. 2). Vertically, As has mainly been detected in groundwater at 5–14 m depth with the highest concentrations at around 10 m depth (i.e. depth of the deep excavation), whereas very low concentrations ($<10 \mu\text{g L}^{-1}$) has been observed in shallower (above 5 m) and deeper zones (below 14 m). The current study focuses on the depth range where the majority of the plume is located.

3. Methodology

3.1. Overall strategy and data evaluation

A range of hydrological and geochemical parameters were measured and analyzed to enable understanding of main factors influencing the long-term As mobilization in the aquifer. To evaluate As mobility including its solid-liquid partitioning at different scales, the following strategy was applied: 1) inverse modelling (IM) of As transport by calibrating a reactive transport model to match long-term field observations of As spreading in the aquifer downstream of the main source area, generating a field-scale “effective K_d ” ($K_{d(IM)}$); 2) evaluation of in-situ As concentrations in paired samples of soil and groundwater, including calculation of local field K_d values in groundwater (GW) at individual sampling points ($K_{d(GW)}$); 3) batch equilibrium tests under oxic conditions performed with the collected soil samples, generating laboratory-oxic (LO) K_d values ($K_{d(LO)}$); 4) generation of laboratory-anoxic (LA) K_d values ($K_{d(LA)}$) corresponding to field conditions using a geochemical model calibrated on data from the batch tests. Results obtained from the different methods were compared and interpreted, with the aim to clarify methodological robustness and potential scaling effects on estimated K_d and the field-scale transport of As. Furthermore, the potential systematic biases in As mobilization-retardation estimation associated with different statistical measures were investigated, considering arithmetic averaging (relevant for non-skewed distributions of flow and transport parameters), geometric averaging (relevant for the skewed log-normal distribution that point samples of K or K_d can display; Persson et al., 2011; Sanchez et al., 2006), and harmonic averaging (e.g., yielding representative K -values in layered or strongly anisotropic media when the main flow direction is perpendicular to the layers; Bear, 1975; Sanchez et al., 2006).

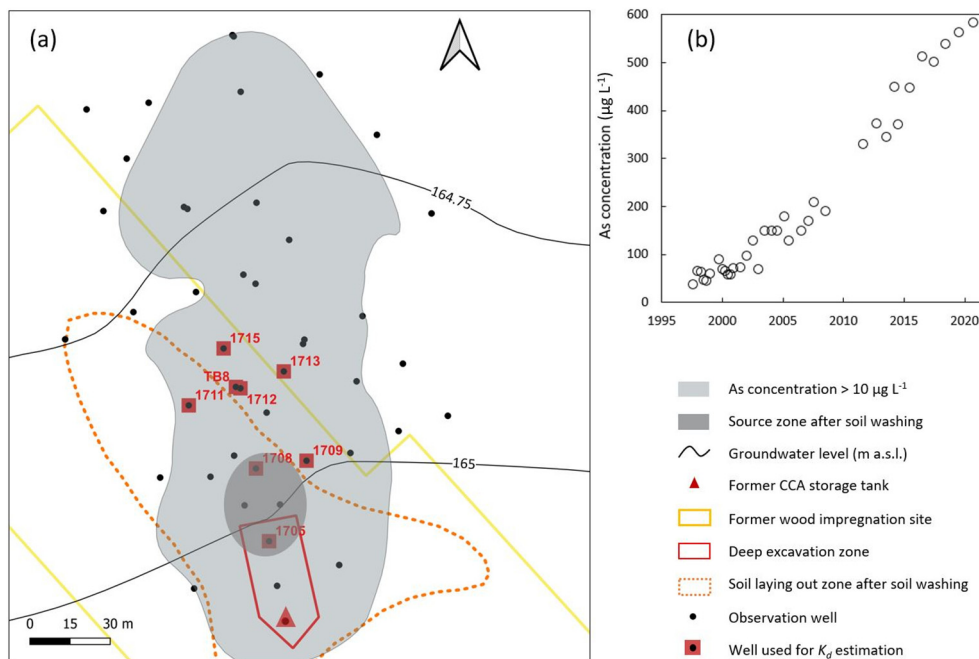


Fig. 2.. Arsenic pollution in the study area: (a) As plume delineation, source zone of As after soil washing and location of the observation wells; (b) Observed As concentration in well TB8 from 1997 to 2021.

3.2. Sampling and analysis

Soil samples (1 m soil cores) were collected in 2017 by vibration drilling (Rotasonic) in seven sampling points well spatially distributed within and downstream of the current source zone (1705, 1708, 1709, 1711, 1712, 1713 and 1715; Fig. 2) at 7–14 m depth, i.e. the depth where the majority of As plume was located. The total As content in soil samples was analyzed by ICP-SFMS after digestion with 7 M HNO_3 . The concentrations of poorly crystalline Fe and Al (hydr)oxides in soil as well as the “geochemically active” fraction of As (i.e. the fraction participating in adsorption/desorption processes) were estimated by oxalate extraction of dried and sieved sediment according to ISO 12782-3 (ISO, 2012). The oxalate extractable As was used to represent the solid-phase concentration in all K_d calculations in this work. The total organic carbon (TOC) in soil was determined by combustion after inorganic carbon (TIC) being removed by acid (EN 13137–2001).

For groundwater sampling, polyethylene pipes with 1 m screens were installed at the corresponding depths of the soil samples. Groundwater levels were measured with light-acoustic-solder and water samples were collected by an electrical submersible pump each autumn from 2017 to 2021, except in wells 1712 and 1713 that were not sampled in 2021. During all the sampling campaigns, redox potential and pH of groundwater were measured in the field with a WTW pH/ORP meter. Groundwater samples for analysis of total concentrations of As, Ca, K, Mn, Mg and P were filtered through 0.45 μm single-use filters in the field, preserved with 1 % HNO_3 and analyzed with Inductively Coupled Plasma (ICP) sector field mass spectrometry or ICP atomic emission spectroscopy. For determination of As(III), groundwater was passed through an As speciation cartridge (MetalSoft Center) and preserved with 1 % HNO_3 prior to analysis with ICP. Dissolved organic carbon (DOC) was analyzed by catalytic combustion and infrared detection after removal of inorganic carbon, P-PO_4 by ammonium molybdate spectrometric method and alkalinity by titration with HCl to pH 5.4. All analyses were performed at a quality accredited laboratory (ISO/IEC 17025:2005).

Slug tests were performed in 2017 and 2018 at 9 test points within the level range of 6–16 m to determine the hydraulic conductivity (K) at different depth. The tests were carried out using Geoprobe's slug test kit and both rising head and falling head tests were conducted at each point. The

obtained data were analyzed using the mathematical model by Hvorslev (1951). For grain size analysis, vertical core samples of 1.5 m length were taken from 4 sampling points, together covering the level range of 2.8–16.8 m. Grain size distributions of borehole sediments were determined by sieve analysis. The result was used for K estimation based on Gustafson's empirical equation (Gustafson, 1983):

$$K = E(u) \cdot d_{10}^2 \quad (1)$$

where d_{10} is the particle size (mm) < 10 % of the sample volume and $E(u)$ is a function of d_{10}/d_{60} . The Gustafson's equation was used since it is a general method which depends solely on the grain size distributions and is well adapted to glaciofluvial deposits (Kitterød, 2008). In addition, the validity of Gustafson's equation has been confirmed by a number of previous studies (e.g., Alfnes et al., 2004; Al-Salem et al., 2020; Lind, 1999).

3.3. Inverse reactive modelling of As transport

The inverse reactive modelling of As transport was based on the Advection-Dispersion-Reaction (ADR) equation. We depart from the fact that the advective breakthrough for inert substances per definition occurs at time t :

$$t = \frac{L}{v} = \frac{L \cdot n_e}{K \cdot I} \quad (2)$$

where L is the distance from the source zone, v is the downgradient average pore water velocity, K is the hydraulic conductivity, I is the hydraulic gradient and n_e is the effective porosity. The basic methodological principle used in this work is that, if the advective – dispersive transport properties of an aquifer are known along with the source concentration (C), the retardation factor (R) describing the net retardation of reactive substances due to their sorption on soil particles can be back-calculated by curve-fitting to an observed breakthrough curve, as illustrated from the analytical solution of the 1D ADR equation (see Supplementary). Assuming equilibrium, R can be related to K_d as (Gillham et al., 1984; U.S. EPA, 1999):

$$R = 1 + \frac{K_d \rho_b}{n_e} \quad (3)$$

where ρ_b is the bulk density and n_e is the effective porosity. The analytical solution also showed that K and C are key variables governing the inverse modelling estimates of R and K_d , whereas the dispersion coefficients have smaller impacts on the results within their well-established possible range.

Practically, the 3D reactive transport of As in the Hjäältevad aquifer was simulated numerically, coupling the groundwater flow model MODFLOW (Harbaugh, 2005) and the solute transport model MT3DMS (Bedekar et al., n.d.) within GMS 10.4 (Aquaveo, 2007). The general transport parameters used in the numerical model are summarized in Table 1. A map of the model domain and grid distribution is shown in Supplementary. Constant head BC (boundary condition) was assigned for the Brusaån River (outlet of the model). No-flow BC was used for the two long sides of the model domain, which were roughly along the direction of groundwater flow. Constant-flux BC was assumed for the inlet of the model, representing groundwater inflow from upstream. The groundwater flow was calibrated by adjusting the groundwater inflow at the inlet of the model to achieve a close fit with the observed groundwater level data. The source zone (Fig. 2) extended throughout model layer 2, 3 and 4. The source concentrations (C_0) were obtained from the average As concentrations measured in four wells in 2017 within the source zone, considering that previous measurements from 1997 have showed essentially time-invariant As concentrations within the source zone.

A sensitivity analysis has showed that the parameter uncertainty related to the dispersivity had limited influence on the simulation of As transport (see details in Supplementary, section 5). The chosen values of dispersivities are shown in Table 1. To investigate the influence of the two key input parameters (K and C), we considered ranges corresponding to plus/minus one standard deviation (σ_K and σ_C) of the mean measurement values (K_0 and C_0) in the main model layer (layer 3), hence with considered $K_{max} = K_0 + \sigma_K$, $C_{max} = C_0 + \sigma_C$, $K_{min} = K_0 - \sigma_K$, and $C_{min} = C_0 - \sigma_C$. This resulted in nine scenarios ($\{K_{max}; C_{max}\}$, $\{K_{max}; C_0\}$, $\{K_{max}; C_{min}\}$, $\{K_0; C_{max}\}$, $\{K_0; C_0\}$, $\{K_0; C_{min}\}$, $\{K_{min}; C_{max}\}$, $\{K_{min}; C_0\}$, $\{K_{min}; C_{min}\}$). For each scenario, the “best fit” inverse modelling estimates of K_d ($K_{d(IM)}$) fitted to the As breakthrough curve at TB8 (Fig. 2b) were obtained by calculating the minimum normalized root mean square error (NRMSE) with a discretization step of 0.1 L kg^{-1} . The calibration was performed based on layer 3 (8–11 m depth), in line with the sampling depth of TB8. This layer corresponds to the most contaminated depth where most of the soil samples were taken, making the derived $K_{d(IM)}$ and the related R -values (Eq. (1)) representative for the plume-scale and comparable with K_d estimated from other methods.

3.4. Batch tests under oxic conditions

Soil samples were air dried at 40°C for 5–7 days to ensure that all As was oxidized to As(V) before being subjected to batch tests according to EN 14429. This approach is practically much more convenient compared

to sampling and handling samples under anoxic conditions. Furthermore, it gave us the possibility to investigate whether it was possible to test the ability of a geochemical model calibrated on oxic conditions to predict the solubility and speciation of As at anoxic field conditions. Ten grams of dried soil ($< 2 \text{ mm}$) and 100 mL leaching solution were added to polypropylene centrifuge tubes (e.g. liquid-to-solid ratio 10). The ionic strength and pH of the leaching solution were adjusted by adding appropriate amounts of NaNO_3 , HNO_3 and/or NaOH to cover a pH range from 4.5 to 9 and to obtain a final NO_3^- concentration of 0.01 mol L^{-1} . The suspensions were equilibrated in an end-over-end shaker for 5.5 days at 21°C in the dark. After equilibration, the samples were centrifuged for at least 20 min at 2500 rpm. The pH of the supernatant was measured and the remaining sample was filtered through $0.45 \mu\text{m}$ single-use filters for analysis of Ca, K, Al, Fe, P- PO_4 and DOC using the same methods as for groundwater (see Section 3.2). K_d representing oxic conditions ($K_{d(LO)}$) was calculated as the ratio of oxalate extractable As in soil to the As concentration in leachates of the batch tests without pH adjustment.

3.5. Geochemical modelling of As partitioning

The solid-liquid partitioning of As was simulated with the software Visual MINTEQ (Gustafsson, 2013), accounting for the aqueous speciation, adsorption/desorption by Fe/Al-(hydr)oxides and binding of cationic elements to solid organic matter (SOM). The concentrations of sorbents and As taking part in equilibrium reactions were estimated from oxalate extractable concentrations in soil samples. A detailed description of model parameters and input data for simulation of As partitioning in the batch tests under oxic conditions can be found in Supplementary. As the concentration of binding sites of Al/Fe (hydr)oxides are affected by different ageing processes, which decreases their sorption potential (Dale et al., 2015; Vu et al., 2013), the concentrations of active Fe/Al-(hydr)oxide sorbents in each soil sample were calibrated using results of the batch tests under oxic conditions, considering all As as As(V). The calibrated model was then used to simulate As partitioning under field conditions. To do this, the As(V)/As(III) redox couple was introduced into the model. Data from groundwater samples from 2017 to 2021 were used as model input, including pH, alkalinity, redox potential, DOC and element concentrations (see Section 4.3).

4. Results and discussion

4.1. Hydraulic conductivity (K) from slug test and grain size distribution

The hydraulic conductivity (K) values obtained from slug tests varied from 4 to 80 m d^{-1} , with higher values close to the ground surface and lower values deeper into the soil (Fig. 3), which was consistent with the decreasing proportion of coarse grain towards depth. The K values calculated

Table 1
Parameters used in the numerical groundwater model MODFLOW and MT3DMS.

Model	Parameter	Value	Comments
General model parameters	Grid size (x direction)	5 m	Horizontally (x, y), the model domain extends from the wood preservation facility to the natural recipient (Brusaån River); vertically (z), the model extends from the ground surface (assumed to be flat) to a depth of 28 m (average bedrock depth).
	Grid size (y direction)	5 m	
	Grid size (z direction)	See Table 2	
	Number of columns (x)	40	
	Number of rows (y)	120	
MODFLOW	Number of layers (z)	6	
	Porosity	0.32	Porosity of medium sand from Morris and Johnson (1967)
	Hydraulic conductivity (K)	See Table 2	Estimated from results of slug tests and grain size distribution
MT3DMS	Aquifer recharge	250 mm year^{-1}	Literature value for the Hjäältevad region from Evehorn et al. (2017)
	Source concentration of As (C)	878, 1582 and $141 \mu\text{g L}^{-1}$ for layer 2, 3 and 4	Estimated from the average As concentrations within the source zone
	Longitudinal dispersivity ^a	1.5 m	Rockhold et al. (2016); Rosenberg et al. (2023); Schulze-Makuch (2005); Zech et al. (2023)
	Transverse dispersivity ^a	Horizontal: 0.03 m; vertical: 0.003 m	Prommer et al. (2006); Rosenberg et al. (2023); Zech et al. (2023)
	Molecular diffusion coefficient	$1.0 \times 10^{-4} \text{ m d}^{-1}$	Tanaka et al., (2013)
	Dry bulk density	1720 kg m^{-3}	Density of quartz material

^a Details regarding the selection of dispersivity values can be found in Supplementary.

from grain size distribution also showed a wide range with an overall decreasing trend towards depth (Fig. 3), in line with the results from slug tests. Considering the non-normal distribution of the data, the natural log transformation (\ln) was performed on all K data and a fairly good linear correlation was derived between $\ln(K)$ and depth:

$$\ln(K) = -0.2 \cdot Z + 4.95 \quad (R^2 = 0.49, P = 4.6 \cdot 10^{-8}) \quad (4)$$

where Z is the depth and R^2 the coefficient of determination. Using Eq. (3), each model layer was assigned an average K -value by back transforming the mean of $\ln(K)$ values within the depth range of each layer to the original scale, which actually corresponded to the definition of geometric mean. We note that the results from the correlation equation differed slightly from the layer-specific geometric mean values calculated from the measurement data within each layer (Table 2), as the former considered global data at all depths while the latter only involves data within each layer. The correlation allowed to calculate K values for all model layers, including layers with few/no data, which were used as input into the numerical model (i.e. K_0).

4.2. Travel times and inverse model (IM) estimates of R and K_d (IM)

Fig. 4a shows three estimates of the breakthrough curves for advective (non-retarded) substance transport (orange lines) from the source zone to the observation well TB8, for comparison with the observed and considerably retarded transport of As (Fig. 4b). Considering conditions in layer 3 (the most polluted aquifer layer), the different possible advective breakthrough curves shown in Fig. 4a reflect that the average (effective) K -value of layer 3 (K_0) is uncertain due to the K -variability within the layer (Fig. 3). We then considered a reasonable K -value range as being $K_0 \pm \sigma_K$ (see the Methodology section), where K_0 and σ_K were found to equal 22 m d^{-1} and 7 m d^{-1} , respectively. The slowest breakthrough (0.94 years; dotted line) hence corresponds to an estimated reasonable minimum K (15 m d^{-1}), whereas the fastest breakthrough (0.51 years) corresponds to a reasonable maximum K (29 m d^{-1}). Similarly, a reasonable C -value ranges was considered as $C_0 \pm \sigma_C$, with C_0 and σ_C equal to $1582 \mu\text{g L}^{-1}$ and $791 \mu\text{g L}^{-1}$, respectively. Considering also dispersion effects, the blue curves of Fig. 4a show corresponding realistic estimates of

Table 2

Depth and hydraulic conductivity for different layers in the numerical model. Numbers within parentheses are geometric standard deviations.

Layer	Depth of layer top (m ^a)	Depth of layer bottom (m ^a)	K from correlation (K_0) (m d ⁻¹)	K from layer-specific geometric mean (m d ⁻¹)
1	0	5	86	106 (1.8)
2	5	8	39	38 (1.7)
3	8	11	22	18 (2.2)
4	11	14	12	11 (2.5)
5	14	19	6	9 (2.1)
6	19	28	1	–

^a m below the ground surface, which is assumed to be flat in the study area.

the (rapid) breakthrough of inert substances in the considered part of the Hjaltevad aquifer.

Compared to such relatively rapid breakthrough of inert substances under the prevailing aquifer conditions in Hjaltevad (Fig. 4a), the observed, actual breakthrough of As in TB8 occurred more gradually at a much slower pace (Fig. 4b; open circles), due to the retardation effects related to sorption. Given our “best estimate” of the key input parameters (K_0 , C_0), the inverse modelling (Table 3) shows that a K_d (IM) -value of 13.6 L kg^{-1} is needed to get a sufficiently high retardation ($R = 74$) that matches the field observations (Fig. 4b, solid curve). Note that there was a general background concentration of As ($60\text{--}80 \mu\text{g L}^{-1}$) at TB8 at start of the simulations, probably due to historical diffuse leaching prior to the remediation performed 1997 (Section 2.2). Given that the actual (effective) K_0 and C_0 are within one standard deviation of this “best estimate”, corresponding K_d (IM) values are within the range 4.9 to 26.3 L kg^{-1} and R within the range 27 to 142 (Table 3), i.e. $27\text{--}142$ times slower than the advective water velocities. The very low minimum NRMSE values (< 0.1) (Table 3) imply that these results are based on good fits between observed and modeled concentrations for each scenario. The $\{K_{max}; C_{max}\}$ scenario combination yields the highest K_d and R values (Table 3), which is consistent with the fact that stronger sorption and retardation of As are needed to match the observations in a case with fast advective transport and high initial concentrations. Fig. 4c illustrates the extent of As plume in layer 3 in 2021 derived from the numerical modelling (base scenario $\{K_0; C_0\}$) compared with field data, showing that the numerical model overall well reproduced the field observations, i.e. use of the K_d (IM) value from inverse modelling provided a good estimation of As transport. Nevertheless, the observed As plume is more heterogeneous than the modeled plume.

4.3. Groundwater geochemistry

Selected chemical parameters of groundwater samples in the 7 wells used for K_d estimation (Fig. 2) are shown in Table 4. Groundwater pH values varied from 5.7 to 7.3 (average 6.4), showing a neutral-weekly acidic environment of the aquifer. The redox potential (Eh) varied both spatially (among sampling points) and temporally (among sampling years), ranging from -270 to 264 mV . The Eh and pH values of groundwaters from these 7 wells are consistent with those of the 32 monitoring wells included in this study (Fig. 5a), suggesting that they are representative for general conditions at the study site. As illustrated in Fig. 5a, anoxic conditions prevailed in the whole aquifer. The low measured Eh values are supported by the generally high concentrations of dissolved Fe in groundwater (Table 4). Data show that Fe concentrations increased drastically at $\text{Eh} < 100 \text{ mV}$ (Fig. 5b), which agrees with an expected reductive dissolution of Fe (hydr)oxide mineral(s) (Schwertmann, 1991). As indicated in Fig. 5c, the Eh in the aquifer was probably buffered by such a process. Although no analytical speciation of Fe was performed on groundwater samples, soluble Fe was very likely dominated by Fe^{2+} in the majority of samples, as low solubility of Fe^{3+} can be expected at near neutral pH values (Menting, 1994). The concentration of dissolved organic carbon (DOC) ranged from 2.0 to 3.6 mg L^{-1} (average 2.8 mg L^{-1}). Anoxic conditions

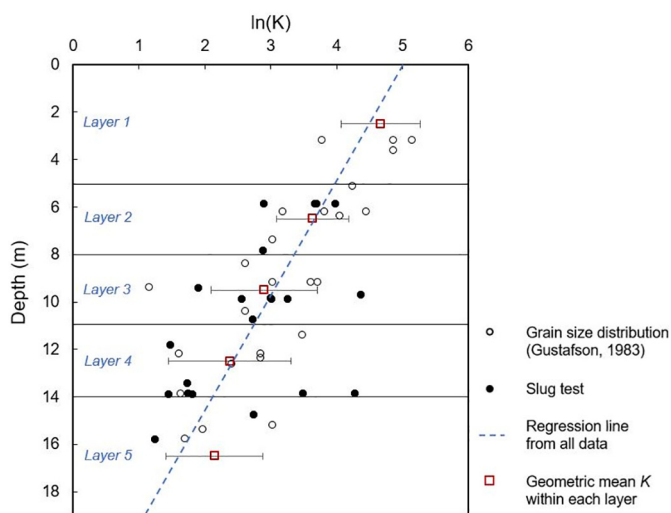


Fig. 3. Relationship between depth and hydraulic conductivity estimated from grain size analyses and slug tests. For deriving the vertical trend (dashed line) as well as the K -value variation within the model layers, the test data were discretized according to which model layer they represented. The middle level of each 1.5 m sampling (test) interval was used for data plotting. Error bars were added, showing the geometric standard deviations for the calculated geometric mean values within each layer.

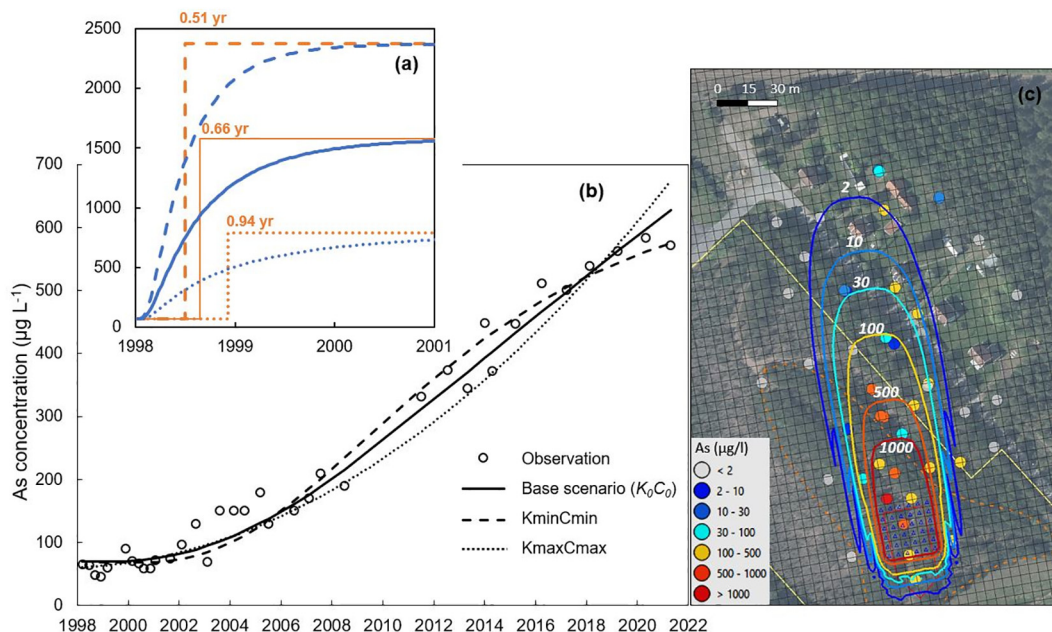


Fig. 4. (a) Advective transport (orange lines) and advective-dispersive transport (blue lines) from the source zone to TB8 without considering adsorption of As to solid-phase materials; (b) Observed As concentration at TB8 vs modeled results considering advection and adsorption of As; (c) modeled As plume in 2021 in layer 3 compared with field measurements in groundwater wells in 2021. The line format corresponding to scenarios are the same in (a) and (b).

also occurred upstream the contaminated area and seems to be the natural state of the aquifer, probably due to input of dissolved organic matter from forests in the watershed. Total As concentrations were generally high in groundwater, ranging from 143 to 1450 $\mu\text{g L}^{-1}$ (average 593 $\mu\text{g L}^{-1}$; Table 4). Analytical speciation of As showed that As(III) was the major form in groundwater (average 538 $\mu\text{g L}^{-1}$), representing 91 % of the average total As concentration. This is in accordance with what could be expected from thermodynamics, as the vast majority of samples are within the As(III) (H_3AsO_3) domain (Fig. 5a). In some samples the measured As(III) concentrations were somewhat higher than the total As concentrations (15 %), which could be attributed to analytical uncertainties in As measurements.

4.4. Field estimates of local K_d values ($K_d(GW)$)

Field local K_d values ($K_d(GW)$) were calculated based on measured As concentrations in paired samples of soil and groundwater (Table 5). On average, the oxalate extractable fraction of As constituted about 70 % of the total As, showing that the selection of total or oxalate extractable content as a measure for solid-phase As only had a moderate influence on K_d evaluations in our dataset. A general high mobility of As in groundwater was highlighted by the relatively low $K_d(GW)$ values. This is consistent with the anoxic conditions in the aquifer, which favors the existence of As in the form of mobile H_3AsO_3 (Smedley and Kinniburgh, 2013). Fig. 5d shows that $K_d(GW)$ values increased with increasing Eh, as expected from the relative stability of the two As species. Further, the $K_d(GW)$ values varied both spatially and temporally. $K_d(GW)$ values differed up to about 2 orders of magnitude, from 1 to 107 L kg^{-1} , between sampling points (illustrating spatial variation), whereas the relative standard

deviation (RSD) at individual sampling points ranged from 4 % to 57 % of the average (illustrating temporal variation). This is consistent with the large local K_d variations as shown in previous studies (Allison and Allison, 2005; Baes III and Sharp, 1983). The overall average $K_d(GW)$ calculated with different averaging methods resulted in values ranging from 3.6 L kg^{-1} (harmonic average) to 38 L kg^{-1} (arithmetic average).

4.5. Batch tests and geochemical modelling, $K_d(LO)$ and $K_d(LA)$

At pH values corresponding to field conditions, As concentrations in eluates of the batch tests were much lower than those observed in groundwater (Fig. 6). Accordingly, $K_d(LO)$ values were much higher than $K_d(GW)$ (Table 5), which is consistent with an oxic system dominated by As(V). As shown in Fig. 6, the solubility of As was strongly pH dependent under oxic conditions, with increasing solubility at increasing pH, which can be explained by the stronger adsorption of As(V) to Fe/Al-(hydr)oxides at lower pH (Anderson and Malotky, 1979; Manning and Goldberg, 1996). Using results of the batch tests, the geochemical model was calibrated by optimizing the concentrations of adsorbing Fe/Al (hydr)oxides, assuming all As to be As(V). The optimized concentrations of (hydr)oxides (HFO_{act}) ranged from 5 to 40 % of the oxalate extractable Fe/Al-(hydr)oxides (Table S2 in Supplementary). The pH dependency of As solubility was generally well reproduced by the model under oxic conditions.

To simulate As partitioning in groundwater 2017–2021, the model was run with groundwater data from field measurements (Table 4). A much closer agreement with groundwater observations was obtained (Fig. 6) and $K_d(LA)$ values were much closer to $K_d(GW)$ than $K_d(LO)$ (Table 5). For 1713, there was an excellent agreement between modeled and measured

Table 3

Scenario summary with calibrated $K_d(IM)$ (L kg^{-1}) and R values. Numbers within parentheses are minimum NRMSE values. The K and C values presented here correspond to layer 3, where the model calibration was performed.

	$C_{min} = 791 \mu\text{g L}^{-1}$	$C_o = 1582 \mu\text{g L}^{-1}$	$C_{max} = 2373 \mu\text{g L}^{-1}$
$K_{min} = 15 \text{ m d}^{-1}$	$K_d = 4.9 (0.05) \rightarrow R = 27$	$K_d = 8.3 (0.06) \rightarrow R = 46$	$K_d = 10.8 (0.07) \rightarrow R = 59$
$K_o = 22 \text{ m d}^{-1}$	$K_d = 7.5 (0.05) \rightarrow R = 41$	$K_d = 13.6 (0.05) \rightarrow R = 74$	$K_d = 18.9 (0.06) \rightarrow R = 103$
$K_{max} = 29 \text{ m d}^{-1}$	$K_d = 10.7 (0.05) \rightarrow R = 59$	$K_d = 20.3 (0.05) \rightarrow R = 110$	$K_d = 26.3 (0.06) \rightarrow R = 142$

Table 4

Groundwater chemistry in wells used for K_d estimation (2017–2021). The data was used in the geochemical model Visual MINTEQ for the simulation of As partitioning under field anoxic conditions. -: not measured.^c

Well	Year	pH	Eh mV	As(tot)	As(III)	Fe	Mn	Ca	K	Mg	Alk ^{a,b}	Cl ^a	SO ₄ ^a	PO ₄ ^a	DOC ^a
				$\mu\text{g L}^{-1}$	$\mu\text{g L}^{-1}$	mg L^{-1}	mg L^{-1}	mg L^{-1}							
1705	2017	5.7	107	812	137	4.4	0.54	11.4	5.6	3.1	28	4.8	10.2	3.6	3.6
	2018	5.9	136	270	82	1.3	0.46	9.9	5.3	3.0	–	–	–	1.9	–
	2019	5.7	264	196	–	0.9	0.41	10.8	5.9	3.4	–	–	–	1.7	–
	2020	6.0	–12	528	141	2.1	0.32	9.3	5.3	2.5	–	–	–	3.2	–
	2021	6.0	92	514	–	2.8	0.35	10.1	5.6	2.8	–	–	–	3.0	–
1708	2017	6.8	–10	1450	1340	5.6	0.59	19.6	2.7	3.1	59	4.9	15.0	2.7	3.4
	2018	6.3	90	856	954	1.3	1.15	22.0	3.9	3.4	–	–	–	1.9	–
	2019	6.2	228	484	–	0.5	1.97	15.4	7.1	3.1	–	–	–	1.5	–
	2020	6.3	60	827	846	1.3	0.95	19.8	3.6	3.1	–	–	–	2.2	–
	2021	6.4	44	721	–	0.1	0.72	18.9	5.4	3.4	–	–	–	2.0	–
1709	2017	6.5	–94	321	251	18.0	0.64	16.5	1.6	2.6	38	6.0	21.5	12.1	2.4
	2018	6.6	–6	361	377	9.2	0.75	14.7	3.7	2.5	–	–	–	7.9	–
	2019	6.3	2	143	–	8.7	0.59	14.0	2.3	2.5	–	–	–	5.4	–
	2020	6.3	–95	310	299	13.0	0.57	14.4	3.0	2.7	–	–	–	10.2	–
	2021	6.4	92^c	150	–	4.7	0.91	15.4	3.4	2.7	–	–	–	10.0	–
1711	2017	7.3	–129	234	204	17.4	1.34	35.7	1.4	3.9	100	5.6	21.0	7.3	2.6
	2018	7.0	–26	192	180	18.2	1.10	35.1	1.5	3.8	–	–	–	5.5	–
	2019	6.4	–50	150	144	12.6	1.29	31.7	1.2	3.9	–	–	–	1.3	–
	2020	7.2	–270	340	262	16.3	1.56	36.0	1.2	4.0	–	–	–	7.8	–
	2021	7.3	1^c	233	–	12.1	1.53	35.3	1.1	3.9	–	–	–	7.0	–
1712	2017	6.5	–7	803	638	9.9	1.00	15.1	2.1	2.9	41	3.8	17.4	7.0	2.0
	2018	6.4	32	551	527	8.8	0.97	13.3	1.7	2.5	–	–	–	9.1	–
	2019	6.1	27	564	–	9.2	0.78	13.8	2.0	2.5	–	–	–	8.5	–
	2020	6.4	136^c	689	632	8.9	0.18	15.0	1.9	2.5	–	–	–	9.8	–
	2021	6.2	–16	643	537	7.6	0.41	12.8	3.4	2.3	38	3.9	14.6	24.1	3.1
1713	2018	6.0	42	589	675	6.9	0.39	11.8	3.4	2.2	–	–	–	15.2	–
	2019	5.8	62	600	–	7.5	0.93	11.6	4.1	2.1	–	–	–	16.8	–
	2020	5.9	–17	602	614	6.7	0.39	11.2	4.3	2.0	–	–	–	16.8	–
	2017	6.8	–110	718	830	10.0	0.89	29.8	0.8	3.3	83	4.9	19.2	6.6	2.6
	2018	6.8	–5	1090	1190	13.5	0.95	26.6	0.7	3.2	–	–	–	8.4	–
1715	2019	6.6	–42	1180	–	12.3	0.96	26.8	0.8	3.3	–	–	–	8.3	–
	2020	6.8	–176	1190	1250	11.3	0.91	28.4	0.9	3.2	–	–	–	8.3	–
	2021	6.9	40^c	1270	–	0.0	1.07	29.6	1.0	3.3	–	–	–	8.0	–
	Mean	6.4	12	593	538	8.0	0.84	19.4	3.0	3.0	55	4.9	17.0	7.4	2.8
	SD	0.4	106	352	382	5.5	0.41	8.8	1.8	0.6	27	0.8	4.0	5.2	0.6

^a Only analyzed in 2017. For DOC, Cl, Alk and SO₄, the value was then used for all years in geochemical modelling.

^b Alkalinity in ground water, entered in Visual MINTEQ as $\text{mg HCO}_3^- \text{L}^{-1}$.

^c Bold value highlight a considerably higher Eh than the others from the same groundwater wells.

As concentrations for all years. The model also well reproduced the measured data at 1709, 1711, 1712 and 1715, except for one year where the modeled concentration was substantially lower (Fig. 6). These samples had a considerably higher Eh than the others from the same groundwater wells (bold values in Table 4) and an unrealistic combination of high Eh and high As concentration. This can be attributed to methodological challenges in field Eh measurements which are extremely sensitive to dissolved oxygen (e.g., Gezahegne et al., 2007; Grenthe et al., 1992). For instance, the pumping procedure during sampling could make the system susceptible to oxygen intrusion, thus disturbing the Eh measurement (Grenthe et al., 1992). While intrusion of small quantities of oxygen could greatly perturb the Eh measurement, the sampled groundwater (total) As concentrations remains more or less unaltered. Calculations including data for all years result in extremely high RSD (>150 %) and much higher $K_d(LA)$ values, whereas excluding the outliers results in a much closer agreement between $K_d(LA)$ and $K_d(GW)$ (Table 5). At 1705 and 1708, the measured As concentrations were systematically higher than the modeled ones for all years (Fig. 6). The low modeled concentrations were related to the relatively high Eh values (> 100 mV) at these two wells. The high Eh might indicate localized highly conductive zones, where preferential flow pathways through macro-pores and/or fissures favored mixing of water of different origins, e.g., shallow groundwater containing oxygen and anoxic water from deeper zones. Another explanation could be heterogeneities in soil and groundwater chemistry. Small amounts of soil samples were used in the batch tests, which provided the basis for geochemical modelling, while the

measured As concentrations in groundwater involved much larger soil volumes, possibly leading to discrepancies between $K_d(LA)$ and $K_d(GW)$.

4.6. Practical implications

The slug tests and particle size distributions showed that local hydraulic properties (K -values) varied by up to two orders of magnitude (Fig. 3). Nevertheless, through the inverse transport modelling, based on the geometric average K (i.e., K_0 derived from correlation between $\ln(K)$ and Z) plus/minus one standard deviation, we could constrain the plume-scale “effective K_d ” to the range 4.9 to 26.3 L kg^{-1} , with K_0 yielding a “best-estimate” K_d of 13.6 L kg^{-1} (Fig. 7; IM). Similarly to K values, the local $K_d(GW)$ values derived from independent in-situ observations of As concentrations also varied by two orders of magnitude (1 to 107 L kg^{-1}), while averaging (arithmetic, geometric, and harmonic) of the local $K_d(GW)$ values could constrain the “effective K_d ” to the range 3.6 to 38 L kg^{-1} , with the geometric average yielding a K_d of 14.4 L kg^{-1} (Fig. 7; GW). Results for the IM and GW methods are hence highly consistent, especially with regard to the geometric averages.

It has previously been shown that geometric averaging of local hydraulic conductivities (K) yields a representative or “effective” value for heterogeneous, isotropic porous media, whereas arithmetic and harmonic averaging are relevant in highly anisotropic media for the longitudinal and transverse flow directions, respectively (Sanchez et al., 2006). Such systematic assessments are however still lacking regarding the averaging of locally varying K_d values. Our IM and GW method comparison shows, to the

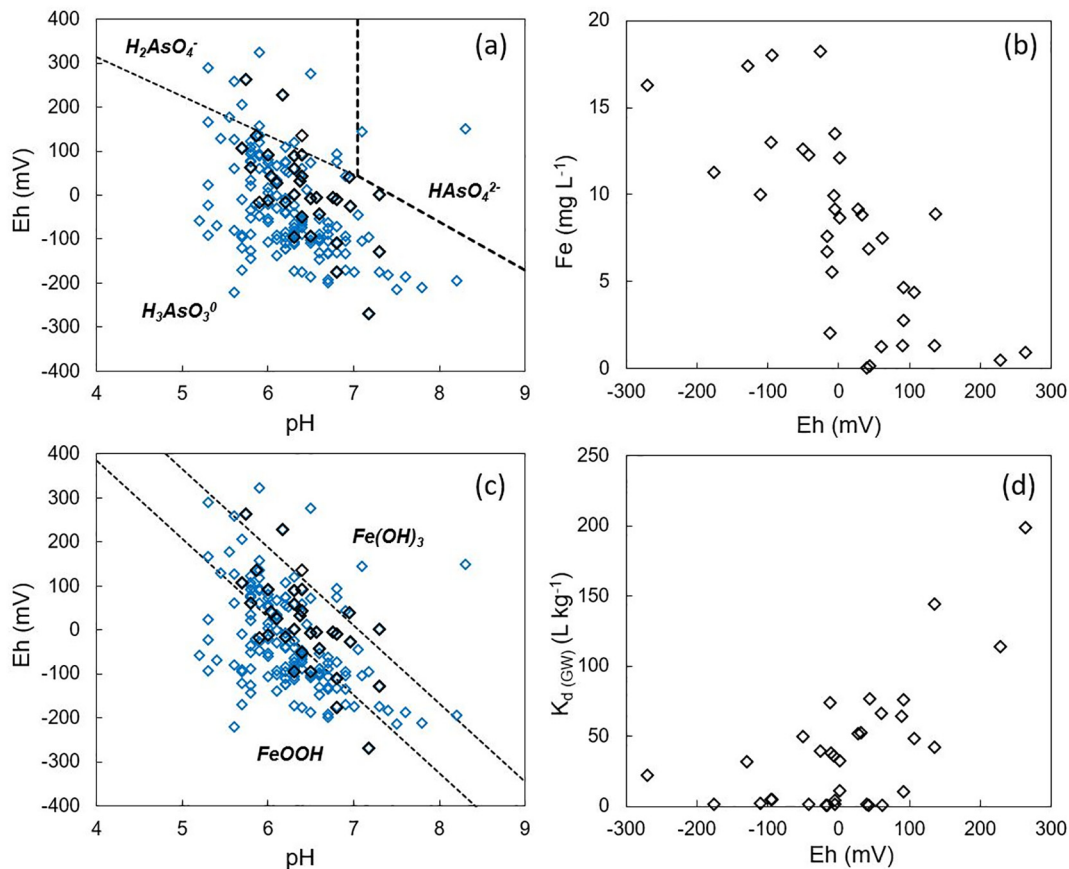


Fig. 5. (a) Stability diagram showing the theoretical relation between As speciation and pH and Eh of groundwater; (b) Relationship between dissolved Fe concentrations and Eh; (c) Stability diagram showing the theoretical relation between Fe speciation and pH and Eh of groundwater; (d) Relationship between $K_{d(GW)}$ and Eh. Black symbols in all diagrams represent samples used for K_d estimation and blue symbols represent samples from other monitoring wells in the study area. Stability lines represent 6 °C and were calculated using thermodynamic data from the data base of Visual MINTEQ, vers. 3.1 (Gustafsson, 2013).

best of our knowledge for the first time, that geometric averaging of local K_d values gives a correspondingly good estimate of “effective K_d ” within heterogeneous, isotropic aquifer layers (such as the studied “layer 3”, which is considered isotropic within the layer, although the whole aquifer shows

variations in the vertical direction). Unless the considered part of the aquifer is strongly anisotropic, we suggest that the geometric average K_d , which has been used in a few previous studies (e.g., Gil-García et al., 2009; Sheppard et al., 2009), will better represent the large-scale “effective K_d ”.

Table 5

As content in solid phase (2017) and groundwater (2017–2021) as well as $K_{d(GW)}$, $K_{d(LA)}$ and $K_{d(LO)}$ values. $K_{d(GW)}$ and $K_{d(LA)}$ at each point are arithmetic averages for 2017–2021. Depth is relative to the original ground surface (+ 168 m a.s.l.) before soil washing; values within parentheses are coefficients of variation (illustrating temporal variation at the sampling point); values within brackets are standard deviations relevant to each averaging method.

Well	Depth		Solid phase		Groundwater		As partition coefficient (K_d)				
	from m	to m	As(tot) mg kg ⁻¹	As(ox) mg kg ⁻¹	As(tot) µg L ⁻¹		$K_{d(GW)}$ L kg ⁻¹	$K_{d(LA)}$ L kg ⁻¹	$K_{d(LO)}$ L kg ⁻¹		
1705	9	10	59	39	464	(52 %)	107	(57 %)	1829	(89 %)	2800
1708	9	10	75	55	868	(41 %)	72	(38 %)	1055	(75 %)	2990
1709	9	10	2.9	1.6	257	(40 %)	7.7	(46 %)	48	(208 %)	970
1711	13	14	15	7.5	230	(31 %)	35	(29 %)	4.0 ^a	(63 %)	1070
									162	(193 %)	
1712	9	10	29	29	652	(18 %)	45	(17 %)	23 ^a	(116 %)	690
									206	(169 %)	
1713	7	8	2.2	0.6	609	(4 %)	1	(4 %)	32 ^a	(79 %)	210
									2.2	(52 %)	
1715	9	10	3.6	1.5	1090	(20 %)	1.4	(26 %)	38	(196 %)	100
									4.8 ^a	(120 %)	
Arithmetic mean							38	[40]	477	[700]	1261 [1173]
Geometric mean							14.4	[6.7]	421 ^a	[723]	744 [3.5]
Harmonic mean							3.6	[2.6]	115	[10]	371 [303]
									35 ^a	[15]	
									13.8	[6.4]	
									7.1 ^a	[6.3]	

^a One outlier excluded for year 2020 (1712) or 2021 (1709, 1711 and 1715) due to likely erroneous Eh measurements.

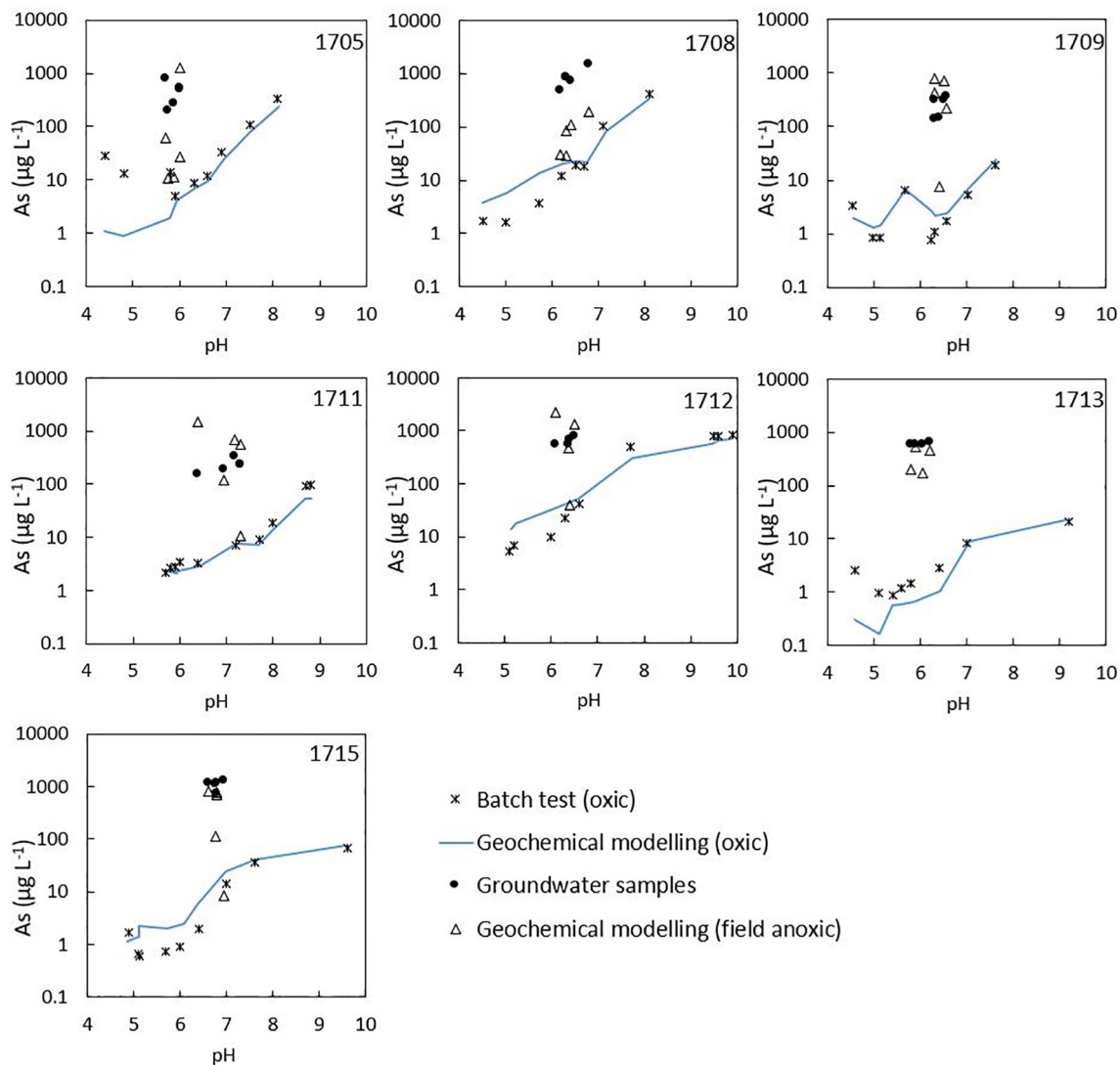


Fig. 6.. As concentrations in groundwater from field measurements (2017-2021), batch tests and geochemical modeling under oxic and field anoxic conditions based on groundwater chemistry in different years.

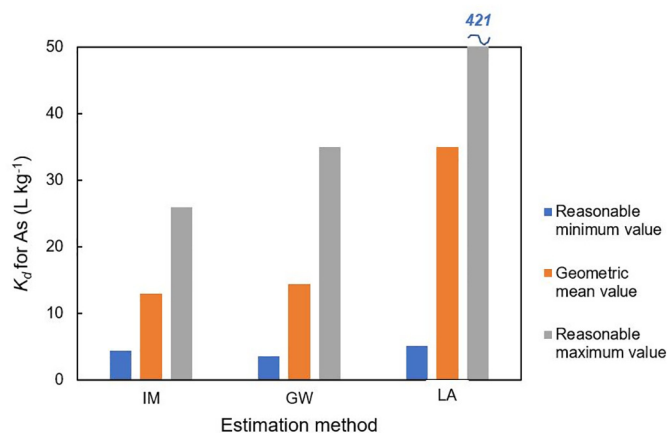


Fig. 7.. Comparison of representative (mean) “Field-K_d” values for As (orange bars) and their reasonable ranges, estimated from different (independent) methods, namely IM: Inverse modelling of observed downstream breakthrough of As, GW: in-situ observations of As concentrations in paired soil-groundwater samples, and LA: geochemical modelling of laboratory-anoxic K_d values.

By analogy of the characteristics of K_d -values, arithmetic averaging of K_d may become more relevant in strongly anisotropic (layered) formations if flow is perpendicular to the layers. Nevertheless, the harmonic averaging of K_d may be relevant in some risk assessment studies, e.g., if a “conservative” value approach is relevant to avoid underestimating the risk.

The good performance of geometric averaging highlights the importance of having a group of point samples whose size is sufficiently large from a statistical perspective to derive an “effective- K_d ” relevant for site-specific assessments of contaminant transport. As shown in our study, geometric mean of K_d based on 7 sampling points was highly consistent with the “effective K_d ” from the inverse modelling, although the range in K_d (GW) varied by two orders of magnitude. Therefore, single or few field measurements of K_d (GW) or K values are very unlikely to be representative of plume-scale effective transport of As (or other metals and metalloids). This may be an important reason behind the generally poor performance of widely used models for predicting groundwater pollution risk at metal contaminated sites (Augustsson et al., 2020), in which case the present study suggests that performance can be considerably enhanced by considering statistically robust sampling strategies, in particular with regard to sample size.

The K_d values derived from the laboratory-anoxic geochemical modelling (LA) exhibited a much larger variability (Table 5) and lower consistency with results from IM and GW. However, geochemical modelling

provided an excellent tool to understand the mechanism of As retention in the Hjältevad aquifer, which relates to the surface complexation of As by Al/Fe (hydr)oxides, impacted by local geochemical variabilities in, e.g. solid-phase concentrations of Fe/Al-(hydr)oxides and groundwater redox potential and pH, explaining the high variability of local K_d values derived from GW. This provides confidence that the K_d values from IM and GW will be long-term valid if the geochemical conditions do not change drastically. Furthermore, the calibrated geochemical model could be used to calculate “equilibrium benchmark values”; i.e. the expected equilibrium As concentrations at a certain groundwater chemistry. At a specific sampling point, deviations from “equilibrium benchmark values” can help to identify non-equilibrium conditions in the groundwater, lab-field scaling issues (representativeness of laboratory samples) and measurement errors, e.g. artefacts related to field measurement of Eh. To ensure that intrusion of small quantities of oxygen does not perturb the Eh measurement, Eh measurements should be supplemented by other redox indicators like As speciation and dissolved Fe concentration.

Our best estimates of K_d for As in the anoxic Hjältevad aquifer (i.e., 13–14 L kg⁻¹, corresponding to a field R of about 80) were comparable with a few existing studies calculating field-based K_d for As under similar aquifer conditions, i.e., suboxic to anoxic environment at neutral pH: 1–8 L kg⁻¹ from Jung et al. (2009) and 5.1–17.3 L kg⁻¹ from Guo et al. (2014). Considering the estimated K_d and R at Hjältevad, the annual distance that the As plume could develop downstream under prevailing conditions is about 0.7 m year⁻¹ (with a pore flow velocity of 57 m year⁻¹). Most anthropogenic As contamination is not older than 50–100 years, corresponding to an expanding distance of about 35–70 m in suboxic to anoxic aquifers. Under such conditions, As plumes can now be expected to gradually cross the borders of industrial areas and pose a risk to downstream water bodies, stressing the urgent need for the remediation of anthropogenic As contaminated sites.

5. Conclusions

From the results of field investigations, laboratory experiments as well as numerical transport modelling at an As-contaminated site from legacy CCA pollution, we concluded that:

- The multi-methodology used in this study, which combines data from local soil and groundwater measurements, batch experiments, chemical equilibrium modelling, and field-scale inverse transport modelling provided an effective and reliable way to understand large-scale mobilization of As in an aquifer.
- The main retention mechanism for As in soil and groundwater at the site is adsorption to surfaces of Fe/Al-(hydr)oxides, which was confirmed by geochemical equilibrium modelling performed on data obtained from laboratory experiments as well as from groundwaters sampled in the field.
- The spatial variation of As partitioning and the local-to-plume scaling issue could be well explained by local heterogeneities in geochemistry and hydrological properties. Our study demonstrated for the first time that geometric averaging of local K_d values gives a good estimate of “effective K_d ” within heterogeneous, isotropic aquifer layers.
- The lab-to-field scaling issue (i.e. discrepancies between $K_{d(LA)}$ and $K_{d(GW)}$) highlighted the potential to use a calibrated geochemical equilibrium model to calculate “equilibrium benchmark values”, i.e. the expected equilibrium As concentrations at a certain groundwater chemistry. This can help to identify non-equilibrium conditions in the groundwater as well as measurement errors, e.g. artefacts related to field measurement of redox potential.

CRedit authorship contribution statement

Feifei Cao: Conceptualization, Formal analysis, Methodology, Visualization, Writing – original draft. **Dan B. Kleja:** Conceptualization, Funding acquisition, Methodology, Project administration, Resources, Supervision, Validation, Writing – review & editing. **Charlotta Tiberg:**

Conceptualization, Formal analysis, Methodology, Visualization, Writing – original draft. **Jerker Jarsjö:** Conceptualization, Funding acquisition, Methodology, Project administration, Resources, Supervision, Validation, Writing – review & editing.

Data availability

Data will be made available on request.

Declaration of competing interest

The authors declare that they have no known competing financial interests or personal relationships that could have appeared to influence the work reported in this paper.

Acknowledgement

This work was funded by Telia company and the TUFFO program – a research and innovation program on contaminated sites managed by the Swedish Geotechnical Institute (SGI) (grant no. 1.1-1905-0340). The authors want to thank Telia company and Peter Englov and Pär Hallgren from Sweco company for their contribution in sampling works and site investigations.

Appendix A. Supplementary data

Supplementary data to this article can be found online at <https://doi.org/10.1016/j.scitotenv.2023.164565>.

References

- Alfnes, E., Kinzelbach, W., Aagaard, P., 2004. Investigation of hydrogeologic processes in a dipping layer structure: 1. The flow barrier effect. *J. Contam. Hydrol.* 69, 157–172. <https://doi.org/10.1016/j.jconhyd.2003.08.005>.
- Allison, J.D., Allison, T.L., 2005. Partition Coefficients for Metals in Surface Water, Soil, and Waste; EPA/600/R-05/074. U.S. Environmental Protection Agency, Washington, DC.
- Al-Salem, S.M., Zeitoun, R., Dutta, A., Al-Nasser, A., Al-Wadi, M.H., Al-Dhafeeri, A.T., Karam, H.J., Asiri, F., Biswas, A., 2020. Baseline soil characterisation of active landfill sites for future restoration and development in the state of Kuwait. *Int. J. Environ. Sci. Technol.* 17, 4407–4418. <https://doi.org/10.1007/s13762-020-02774-1>.
- Andersen, S., Rasmussen, G., Snilsberg, P., Amundsen, C.E., Westby, T., 1996. Assessing toxicity and mobilisation of impregnation salts at a contaminated site. *Fresenius J. Anal. Chem.* 354, 676–680. <https://doi.org/10.1007/s0021663540676>.
- Anderson, M.A., Malotky, D.T., 1979. The adsorption of protolyzable anions on hydrous oxides at the isoelectric pH. *J. Colloid Interface Sci.* 72, 413–427. [https://doi.org/10.1016/0021-9797\(79\)90343-6](https://doi.org/10.1016/0021-9797(79)90343-6).
- Aquaveo, L.L.C., 2007. Groundwater Modeling System Version 6.5. 6, build date, May 27, 2009. UT USA.
- Augustsson, A., Uddh Söderberg, T., Fröberg, M., Berggren Kleja, D.B., Åström, M., Svensson, P.A., Jarsjö, J., 2020. Failure of generic risk assessment model framework to predict groundwater pollution risk at hundreds of metal contaminated sites: implications for research needs. *Environ. Res.* 185, 109252. <https://doi.org/10.1016/j.envres.2020.109252>.
- Baes III, C.F., Sharp, R.D., 1983. A proposal for estimation of soil leaching and leaching constants for use in assessment models. *J. Environ. Qual.* 12, 17–28. <https://doi.org/10.2134/jeq1983.00472425001200010003x>.
- Bear, J., 1975. Dynamics of Fluids in Porous Media. *Soil Sci.* 120, 162–163. <https://doi.org/10.1097/00010694-197508000-00022>.
- Bedekar, V., Morway, E.D., Langevin, C.D., Tonkin, M.J., 2016. MT3D-USGS version 1: a U.S. Geological Survey release of MT3DMS updated with new and expanded transport capabilities for use with MODFLOW (No. 6-A53), Techniques and Methods. U.S. Geological Survey. doi: <https://doi.org/10.3133/tm6A53>.
- Blaisi, N.I., Clavier, K.A., Roessler, J.G., Chung, J., Townsend, T.G., Al-Abed, S.R., Bonzongo, J.-C.J., 2019. Material- and site-specific partition coefficients for beneficial use assessments. *Environ. Sci. Technol.* 53, 9626–9635. <https://doi.org/10.1021/acs.est.9b01756>.
- Carraro, A., Fabbri, P., Giaretta, A., Peruzzo, L., Tateo, F., Tellini, F., 2015. Effects of redox conditions on the control of arsenic mobility in shallow alluvial aquifers on the Venetian Plain (Italy). *Sci. Total Environ.* 532, 581–594. <https://doi.org/10.1016/j.scitotenv.2015.06.003>.
- Charlet, L., Chakraborty, S., Appelo, C.A.J., Roman-Ross, G., Nath, B., Ansari, A.A., Lanson, M., Chatterjee, D., Mallik, S.B., 2007. Chemodynamics of an arsenic “hotspot” in a West Bengal aquifer: a field and reactive transport modeling study. *Appl. Geochem.* 22, 1273–1292. <https://doi.org/10.1016/j.apgeochem.2006.12.022>.
- Chatain, V., Sanchez, F., Bayard, R., Moszkowicz, P., Gourdon, R., 2005. Effect of experimentally induced reducing conditions on the mobility of arsenic from a mining soil. *J. Hazard. Mater.* 122, 119–128. <https://doi.org/10.1016/j.jhazmat.2005.03.026>.

- Cozzarelli, I.M., Schreiber, M.E., Erickson, M.L., Ziegler, B.A., 2016. Arsenic cycling in hydrocarbon plumes: secondary effects of natural attenuation. *Groundwater* 54, 35–45. <https://doi.org/10.1111/gwat.12316>.
- Dale, J.G., Stegemeier, J.P., Kim, C.S., 2015. Aggregation of nanoscale iron oxyhydroxides and corresponding effects on metal uptake, retention, and speciation: I. Ionic-strength and pH. *Geochim. Cosmochim. Acta* 148, 100–112. <https://doi.org/10.1016/j.gca.2014.08.029>.
- Davies, O.R., 2022. Solubility of Arsenic in Untreated and ZVI-Treated Contaminated Aquifer Material. Master thesis, SLU, Dept. of Soil and Environment, Uppsala 50 p.
- Degryse, F., Smolders, E., Parker, D.R., 2009. Partitioning of metals (Cd, Co, Cu, Ni, Pb, Zn) in soils: concepts, methodologies, prediction and applications – a review. *Eur. J. Soil Sci.* 60, 590–612. <https://doi.org/10.1111/j.1365-2389.2009.01142.x>.
- Eveborn, D., Vikberg, E., Thunholm, B., Hjerne, C.E., Gustafsson, M., 2017. Grundvattenbildning och grundvattentillgång i Sverige Uppsala: Sveriges Geologiska Undersökning (SGU:s diarie-nr: 21-2925/2016, RR 2017:0).
- Ganne, P., Cappuyens, V., Vervoort, A., Buvé, L., Swennen, R., 2006. Leachability of heavy metals and arsenic from slags of metal extraction industry at Angleur (eastern Belgium). *Sci. Total Environ.* 356, 69–85. <https://doi.org/10.1016/j.scitotenv.2005.03.022>.
- Gezahegne, W.A., Planer-Friedrich, B., Merkel, B.J., 2007. Obtaining stable redox potential readings in gneiss groundwater and mine water: difficulties, meaningfulness, and potential improvement. *Hydrogeol. J.* 15, 1221–1229. <https://doi.org/10.1007/s10040-007-0174-0>.
- Gil-García, C., Tagami, K., Uchida, S., Rigol, A., Vidal, M., 2009. New best estimates for radionuclide solid-liquid distribution coefficients in soils. Part 3: miscellany of radionuclides (Cd, Co, Ni, Zn, I, Se, Sb, Pu, Am, and others). *J. Environ. Radioact.* 100, 704–715. <https://doi.org/10.1016/j.jenvrad.2008.12.001>.
- Gillham, R.W., Cherry, J.A., Barker, J.F., 1984. *Groundwater Contamination*. National Academy press, Washington D.C. (ISBN 0-309-03441-8.).
- Grenthe, I., Stumm, W., Laaksoharju, M., Nilsson, A.C., Wikberg, P., 1992. Redox potentials and redox reactions in deep groundwater systems. *Chem. Geol.* 98, 131–150. [https://doi.org/10.1016/0009-2541\(92\)90095-M](https://doi.org/10.1016/0009-2541(92)90095-M).
- Guo, Q., Guo, H., Yang, Y., Han, S., Zhang, F., 2014. Hydrogeochemical contrasts between low and high arsenic groundwater and its implications for arsenic mobilization in shallow aquifers of the northern Yinchuan Basin, P.R. China. *J. Hydrol., Arsenic in hydrological processes—Sources, speciation, bioavailability and management* 518, 464–476. <https://doi.org/10.1016/j.jhydrol.2014.06.026>.
- Gustafson, G., 1983. Brunnsystem för värmelagring och värmeutvinning i akviferer. Byggnadsförskningsrådet. Rapport R39:1983. ISBN 91-540-3912-6, Stockholm, Sweden.
- Gustafsson, J.P., 2013. Visual MINTEQ, 3.1 Available at <http://vminteq.lwr.kth.se/>.
- Harbaugh, A.W., 2005. MODFLOW-2005: the U.S. Geological Survey modular ground-water model—the ground-water flow process. *Tech. Methods.* <https://doi.org/10.3133/tm6A16>.
- Hopp, L., Peiffer, S., Durner, W., 2006. Spatial variability of arsenic and chromium in the soil water at a former wood preserving site. *J. Contam. Hydrol.* 85, 159–178. <https://doi.org/10.1016/j.jconhyd.2006.01.005>.
- Hvorslev, M.J., 1951. Time Lag and Soil Permeability in Ground-Water Observations (Report). U. S. Army Engineer Waterways Experiment Station, p. 50.
- ISO, 2012. International Organization for Standardization. (2012). Soil Quality — Parameters for Geochemical Modelling of Leaching and Speciation of Constituents in Soils and Materials — Part 3: Extraction of Aluminium Oxides and Hydroxides With Ammonium Oxalate/Oxalic Acid (ISO 12782-3:2012).
- Jang, Y.-C., Townsend, T.G., Ward, M., Bitton, G., 2002. Leaching of arsenic, chromium, and copper in a contaminated soil at a wood preserving site. *Bull. Environ. Contam. Toxicol.* 69, 0808–0816. <https://doi.org/10.1007/s00128-002-0132-4>.
- Jarsjö, J., Andersson-Sköld, Y., Fröberg, M., Pietroni, J., Borgström, R., Löf, Å., Kleja, D.B., 2020. Projecting impacts of climate change on metal mobilization at contaminated sites: controls by the groundwater level. *Sci. Total Environ.* 712, 135560. <https://doi.org/10.1016/j.scitotenv.2019.135560>.
- Jung, H.B., Charette, M.A., Zheng, Y., 2009. Field, laboratory, and modeling study of reactive transport of groundwater arsenic in a coastal aquifer. *Environ. Sci. Technol.* 43, 5333–5338. <https://doi.org/10.1021/es90080q>.
- Jung, H.B., Bostick, B.C., Zheng, Y., 2012. Field, experimental, and modeling study of arsenic partitioning across a redox transition in a Bangladesh aquifer. *Environ. Sci. Technol.* 46, 1388–1395. <https://doi.org/10.1021/es2032967>.
- Keimowitz, A.R., Simpson, H.J., Stute, M., Datta, S., Chillrud, S.N., Ross, J., Tsang, M., 2005. Naturally occurring arsenic: mobilization at a landfill in Maine and implications for remediation. *Appl. Geochem.* 20, 1985–2002. <https://doi.org/10.1016/j.apgeochem.2005.06.008>.
- Kitterød, N.-O., 2008. Focused flow in the unsaturated zone after surface ponding of snowmelt. *Cold Reg. Sci. Technol.*, Fifth International Conference on Contaminants in Freezing Ground. 53, pp. 42–55. <https://doi.org/10.1016/j.coldregions.2007.09.005>.
- Lind, B.B., 1999. The influence of grain-size and sediment sorting on the hydraulic conductivity of some Swedish tills. *GFF* 121, 107–111. <https://doi.org/10.1080/11035899901212107>.
- Manning, B.A., Goldberg, S., 1996. Modeling competitive adsorption of arsenate with phosphate and molybdate on oxide minerals. *Soil Sci. Soc. Am. J.* 60, 121–131. <https://doi.org/10.2136/sssaj1996.03615995006000010020x>.
- Mariner, P.E., Holzmer, F.J., Jackson, R.E., Meinardus, H.W., Wolf, F.G., 1996. Effects of high pH on arsenic mobility in a shallow sandy aquifer and on aquifer permeability along the adjacent shoreline, Commencement Bay Superfund Site, Tacoma, Washington. *Environ. Sci. Technol.* 30, 1645–1651. <https://doi.org/10.1021/es9506420>.
- Menting, V., 1994. Solubility Studies of Iron(III) Oxides and Hydroxides. Master thesis, Portland State University, Department of Chemistry <https://doi.org/10.15760/etd.6729> 58p.
- Michael, H.A., Khan, M.R., 2016. Impacts of physical and chemical aquifer heterogeneity on basin-scale solute transport: vulnerability of deep groundwater to arsenic contamination in Bangladesh. *Adv. Water Resour.* 98, 147–158. <https://doi.org/10.1016/j.advwatres.2016.10.010>.
- Moras, S., Fonseca, H.M.A.C., Oliveira, S.M.R., Oliveira, H., Gupta, V.K., Sharma, B., de Lourdes Pereira, M., 2021. Environmental and health hazards of chromated copper arsenate-treated wood: a review. *Int. J. Environ. Res. Public Health* 18, 5518. <https://doi.org/10.3390/ijerph18115518>.
- Morris, D.A., Johnson, A.L., 1967. Summary of hydrologic and physical properties of rock and soil materials, as analyzed by the hydrologic laboratory of the U.S. Geological Survey, 1948–60, Water Supply Paper. U.S. Government Printing Office <https://doi.org/10.3133/wsp1839D>.
- Nadiri, A.A., Sadeghi Aghdam, F., Khatibi, R., Asghari Moghaddam, A., 2018. The problem of identifying arsenic anomalies in the basin of Sahand dam through risk-based ‘soft modelling’. *Sci. Total Environ.* 613–614, 693–706. <https://doi.org/10.1016/j.scitotenv.2017.08.027>.
- Nakiguli, C.K., Ojok, W., Omara, T., Wasswa, J., Ntambi, E., 2020. Mobility of Chromium, Copper and Arsenic in Amended Chromated Copper Arsenate Contaminated Soils.
- Ni, P., Guo, H., Cao, Y., Jia, Y., Jiang, Y., Zhang, D., 2016. Aqueous geochemistry and its influence on the partitioning of arsenic between aquifer sediments and groundwater: a case study in the northwest of the Hetao Basin. *Environ. Earth Sci.* 75, 356. <https://doi.org/10.1007/s12665-016-5294-1>.
- Nriagu, J.O., Bhattacharya, P., Mukherjee, A.B., Bundschuh, J., Zevenhoven, R., Loeppert, R.H., 2007. Arsenic in soil and groundwater: an overview. *Trace Metals and Other Contaminants in the Environment, Arsenic in Soil and Groundwater Environment*. Elsevier, pp. 3–60 [https://doi.org/10.1016/S1875-1121\(06\)09001-8](https://doi.org/10.1016/S1875-1121(06)09001-8).
- O'Day, P.A., Vlassopoulos, D., Root, R., Rivera, N., 2004. The influence of sulfur and iron on dissolved arsenic concentrations in the shallow subsurface under changing redox conditions. *Proc. Natl. Acad. Sci.* 101, 13703–13708. <https://doi.org/10.1073/pnas.0402775101>.
- Oremland, R.S., Stolz, J.F., 2003. The ecology of arsenic. *Science* 300, 939–944. <https://doi.org/10.1126/science.1081903>.
- Persson, K., Jarsjö, J., Destouni, G., 2011. Diffuse hydrological mass transport through catchments: scenario analysis of coupled physical and biogeochemical uncertainty effects. *Hydrol. Earth Syst. Sci.* 15, 3195–3206. <https://doi.org/10.5194/hess-15-3195-2011>.
- Prommer, H., Tuxen, N., Bjerg, P.L., 2006. Fringe-controlled natural attenuation of phenoxy acids in a landfill plume: integration of field-scale processes by reactive transport modeling. *Environ. Sci. Technol.* 40, 4732–4738. <https://doi.org/10.1021/es0603002>.
- Rockhold, M.L., Zhang, Z.F., Bott, Y.-J., 2016. Scale-Dependent Solute Dispersion in Variably Saturated Porous Media. No. PNNL-25146. Pacific Northwest National Lab. <https://doi.org/10.2172/1365451> (PNNL), Richland, WA (United States).
- Rosenberg, L., Mosthaf, K., Broholm, M.M., Fjordbøge, A.S., Tuxen, N., Kerm-Jespersen, I.H., Rønne, V., Bjerg, P.L., 2023. A novel concept for estimating the contaminant mass discharge of chlorinated ethenes emanating from clay till sites. *J. Contam. Hydrol.* 252, 104121. <https://doi.org/10.1016/j.jconhyd.2022.104121>.
- Sanchez, C.A., Krieger, R.L., Khandaker, N.R., Valentin-Blasini, L., Blount, B.C., 2006. Potential perchlorate exposure from Citrus sp. irrigated with contaminated water. *Anal. Chim. Acta, Perchlorate: an Enigma for the New Millennium* 567, 33–38. <https://doi.org/10.1016/j.aca.2006.02.013>.
- Saxe, J.K., Wannamaker, E.J., Conklin, S.W., Shupe, T.F., Beck, B.D., 2007. Evaluating landfill disposal of chromated copper arsenate (CCA) treated wood and potential effects on groundwater: evidence from Florida. *Chemosphere* 66, 496–504. <https://doi.org/10.1016/j.chemosphere.2006.05.063>.
- Sbarbati, C., Barbieri, M., Barron, A., Bostick, B., Colombani, N., Mastrociccio, M., Prommer, H., Passarelli, S., Zheng, Y., Petitta, M., 2020. Redox dependent arsenic occurrence and partitioning in an industrial coastal aquifer: evidence from high spatial resolution characterization of groundwater and sediments. *Water* 12, 2932. <https://doi.org/10.3390/w12102932>.
- Schulze-Makuch, D., 2005. Longitudinal dispersivity data and implications for scaling behavior. *Groundwater* 43, 443–456. <https://doi.org/10.1111/j.1745-6584.2005.0051.x>.
- Schwertmann, U., 1991. Solubility and dissolution of iron oxides. *Plant Soil* 130, 1–25. <https://doi.org/10.1007/BF00011851>.
- Sheppard, S., Long, J., Sanipelli, B., Sohlenius, G., 2009. Solid/liquid partition coefficients (Kd) for selected soils and sediments at Forsmark and Laxemar-Simpevarp. ISSN 1402-3091, SKB Rapport R-09-27. Sweden.
- Smedley, P.L., Kinniburgh, D.G., 2002. A review of the source, behaviour and distribution of arsenic in natural waters. *Appl. Geochem.* 17, 517–568. [https://doi.org/10.1016/S0883-2927\(02\)00018-5](https://doi.org/10.1016/S0883-2927(02)00018-5).
- Smedley, P.L., Kinniburgh, D.G., 2013. Arsenic in groundwater and the environment. In: Selinus, O. (Ed.), *Essentials of Medical Geology*, Revised edition Springer, Netherlands, Dordrecht, pp. 279–310 https://doi.org/10.1007/978-94-007-4375-5_12.
- Stockmann, M., Schikora, J., Becker, D.-A., Flügge, J., Noseck, U., Brendler, V., 2017. Smart Kd-values, their uncertainties and sensitivities - applying a new approach for realistic distribution coefficients in geochemical modeling of complex systems. *Chemosphere* 187, 277–285. <https://doi.org/10.1016/j.chemosphere.2017.08.115>.
- Stolze, L., Zhang, D., Guo, H., Rolle, M., 2019. Model-based interpretation of groundwater arsenic mobility during in situ reductive transformation of Ferrihydrite. *Environ. Sci. Technol.* 53, 6845–6854. <https://doi.org/10.1021/acs.est.9b00527>.
- Stopelli, E., Duyen, V.T., Mai, T.T., Trang, P.T.K., Viet, P.H., Lightfoot, A., Kipfer, R., Schneider, M., Eiche, E., Kontny, A., Neumann, T., Glodowska, M., Patzner, M., Kappler, A., Kleindienst, S., Rathi, B., Cirpka, O., Bostick, B., Prommer, H., Winkel, L.H.E., Berg, M., 2020. Spatial and temporal evolution of groundwater arsenic contamination in the Red River delta, Vietnam: interplay of mobilisation and retardation processes. *Sci. Total Environ.* 717, 137143. <https://doi.org/10.1016/j.scitotenv.2020.137143>.
- U.S. EPA, 1999. EPA 402-R-99-004A - Understanding Variation in Partition Coefficient, Kd, Values. Volume I: the Kd Model, Methods of Measurement, and Application of Chemical Reaction Codes. U. S. Environmental Protection Agency, USA.
- van Geen, A., Radloff, K., Aziz, Z., Cheng, Z., Huq, M.R., Ahmed, K.M., Weinman, B., Goodbred, S., Jung, H.B., Zheng, Y., Berg, M., Trang, P.T.K., Charlet, L., Metral, J., Tisserand, D., Guillot, S., Chakraborty, S., Gajurel, A.P., Upreti, B.N., 2008. Comparison

- of arsenic concentrations in simultaneously-collected groundwater and aquifer particles from Bangladesh, India, Vietnam, and Nepal. *Appl. Geochem. Arsenic in groundwaters of South-East Asia: With emphasis on Cambodia and Vietnam* 23, 3244–3251. <https://doi.org/10.1016/j.apgeochem.2008.07.005>.
- Vu, H.P., Shaw, S., Brinza, L., Benning, L.G., 2013. Partitioning of Pb(II) during goethite and hematite crystallization: implications for Pb transport in natural systems. *Appl. Geochem.* 39, 119–128. <https://doi.org/10.1016/j.apgeochem.2013.10.001>.
- Wallis, L., Prommer, H., Berg, M., Siade, A.J., Sun, J., Kipfer, R., 2020. The river–groundwater interface as a hotspot for arsenic release. *Nat. Geosci.* 13, 288–295. <https://doi.org/10.1038/s41561-020-0557-6>.
- Yang, X., Hou, Q., Yang, Z., Zhang, X., Hou, Y., 2012. Solid-solution partitioning of arsenic (As) in the paddy soil profiles in Chengdu Plain, Southwest China. *Geosci. Front. Charnockites and Charnockites* 3, 901–909. <https://doi.org/10.1016/j.gsf.2012.03.006>.
- Zech, A., Attinger, S., Bellin, A., Cvetkovic, V., Dagan, G., Dietrich, P., Fiori, A., Teutsch, G., 2023. Evidence based estimation of macrodispersivity for groundwater transport applications. *Groundwater* 61, 346–362. <https://doi.org/10.1111/gwat.13252>.